Materials Technology Reports 2023; 1(1): 288.
Original Research Article

Effect of the welding procedure on the deformation of superposed welds of a low carbon steel

Rafael Humberto Mota de Siqueira[1], Sheila Medeiros de Carvalho[2], Milton Sergio Fernandes de Lima[1,3,*]

[1] *Photonics Division, Institute for Advanced Studies, 12228-001 São José dos Campos, SP, Brazil*

[2] *Department of Mechanical Engineering, Federal University of Espirito Santo, 29075-910 Vitoria, ES, Brazil*

[3] *Thematic Network in Materials Engineering, Federal University of Ouro Preto, 35400-000 Ouro Preto, MG, Brazil*

*** Corresponding author:** Milton Sergio Fernandes de Lima, msflima@gmail.com

ARTICLE INFO

Received: 1 November 2023
Accepted: 23 November 2023
Available online: 19 December 2023

doi: 10.59400/mtr.v1i1.288

ABSTRACT: This study compared gas-metal arc welding (GMAW) and laser beam welding (LBW) for the superposed joining of two low-carbon steels. The motivation was to reduce the visible defects (notches) in the external part of one of the sheets. Both welding processes produced sound welds characterized by ferrite and pearlite; however, the notch disappeared when LBW was used. The hardness values of the fusion and heat-affected zones were similar for both processes, but the tensile strengths were very different. The shear tensile strengths of the LBW and GMAW were 415 and 84 MPa, respectively. Finite element analysis simulations indicated a more diffuse distribution of the von Mises stress throughout the welded component. The GMAW FEA model also presented a defect because of excessive heat transfer and residual stresses. In conclusion, LBW can replace GMAW in this particular case with improvements in appearance, productivity, and mechanical strength.

KEYWORDS: gas-metal arc welding; laser beam welding; low-carbon steel; automotive

1. Introduction

Several joining techniques have been exploited in the transportation industry and have attained a high level of automation and quality control. For automotive construction, arc, electrical resistance, friction, and laser methods have been widely employed for tailored-blank and body-in-white welds[1]. None of these methods except for minor defects should be considered for the purpose of the component. For example, a small undercut in a mid-floor auto blank can be considered less critical than an inconsistent weld in a door beam. In other cases, the part should attain a cosmetic appearance along with mechanical and metallurgical qualities. For example, this is the case for a truck bumper, which is usually a gas-metal arc weld (GMAW) to a clip in the body frame; however, the external appearance of the bumper should be as flat as possible for aesthetic reasons. These components are sometimes painted black at the end of the manufacturing line, and the appearance of small surface deformations is apparent to the client. In addition to the aesthetic question, GMAW seems to be sufficient to fulfill the requirements of the component during the truck lifetime[2].

In the present work, laser beam welding (LBW) is proposed as a replacement for GMAW for steel bumper clip joining. This replacement aims to overcome the small delamination at the free surface resulting from arc welding, together with enhanced automation potential and process speed. Mechanical tests were performed to evaluate the performance of each method.

A comparison between arc and laser methods has been reported in the literature. Sakai et al.[3] compared GTAW (gas-tungsten arc welding), plasma, and laser sources for the welding of SAE 300 M steel. For the authors, the choice of source did not change the tensile mechanical behavior or hardness.

Antunes and de Lima[4] compared GMAW, laser, and hybrid welding (laser plus GMAW) for the welding of 2.16 mm thick Dual Phase (DP) 600 steel. These authors reported that GMAW is not a suitable route because of the massive tempering of the base material, which results in premature failure. Similarly, both laser and hybrid techniques are recommended according to the microstructure, hardness, and tensile behavior standards.

Hashemzadeh et al.[5] studied the question of finite element models for GMAW and LBW steel sheets. Although the simulations seem to be a good fit to the experimental data, the question of deformation is missing, and according to the authors, a more robust model must be considered.

The novelty aspect of the present contribution concerns the comparison of steel superposed weld coupons from numerical computation results, which provides further robustness to the decision of automakers to consider one method or another.

The residual stresses in laser beam-welded C-Mn steel blanks were considered by Derakhshan et al.[6]. According to these authors, the residual stresses and deformations are linked to the heat input when comparing arc welding to laser welding. Similar results were reported by Pavan for austenitic stainless steels[7].

The objective of the present work is to verify whether laser beam welding (LBW) can replace gas-metal arc welding (GMAW) for superposed welding of 1.9 mm low-carbon steel sheets in terms of final deformations, microstructure, and mechanical behavior.

2. Experimental

A 1.9 mm thick low-carbon steel sheet with a composition of Fe-0.02_{max}C-0.25_{max}Mn-0.01_{max}Al-0.02_{max}P-0.30_{max}Ti (weight %), was used in the as-annealed state. According to the manufacturer, steel has a yield strength (YS) between 140 and 180 MPa, an ultimate tensile strength (UTS) between 270 and 330 MPa, a maximum elongation (ME) of 40%, and a hardness of approximately 48 HRB.

The welds were prepared according to the geometries required for application. GMAW realized a flat-position lap joint using an ESAB source and manual procedures. The arc welding parameters were 17.2 V, 76 A, wire speed of 6.3 mm/s, and argon gas shielding (8 L/min). The OK AristoRod 12.63 ESAB_filler wire (classification EN ISO 14341-A) had a diameter of 0.8 mm and a typical composition (Fe as the balance) of 0.074% C, 1.68% Mn, and 0.95% Si.

For LBW, a Yb:glass fiber laser (IPG Photonics, model YLR-2000) was used. The geometry was superposed sheets with the laser focus on the top of the upper sheet (0.1 mm spot diameter). After some free trials, the laser power was fixed at 1800 W, and the weld speed was 25 mm/s.

The welds were analyzed using an optical microscope (Zeiss, model Axio Imager.A2m) after polishing and etching with a solution of 2% nitric acid in ethanol. The hardness of the different regions was acquired using a FutureTech model FM-700 microhardness tester with a 100-gf load and a dwell time of 10 s. Tensile strength tests were carried out in an Instron universal mechanical testing machine (DL 10'000), with an axial speed of 1 mm/min. Three tensile coupons were tested for comparison purposes.

Finite element analysis (FEA) simulations were performed using Sysweld Software©[8]. Sysweld is

FEA software specially designed for welding and heat treatment of metals and alloys. For the current purpose, a mesh refined around the laser or arc path was designed, and the actual experimental conditions were considered. The material properties in the database were low-carbon steel grade DC04 (1.0338) for both the base sheets and wire.

3. Results and discussion

Figure 1 shows two micrographs of the transverse cut after GMAW and LBW. The GMAW joint, shown in **Figure 1(a)**, has a 5.2 mm wide weld bead with a resolidified material height of 2.8 mm and melts through the lower sheet of approximately 0.4 mm. A pore is perceived at the interface between the sheets, which is due to the pumping of gases into the gap. Large grains around the welded zone are shown in **Figure 1(a)**, owing to the heat input. **Figure 1(a)** also shows an arrow indicating a notch on the external surface of the bottom sheet. The notch dimensions are 0.27 mm wide and 0.03 mm deep, which is relatively small but easily noticed by a visual inspection of the component. **Figure 1(b)** shows an LBW cross-sectional micrograph with a typical heyhole shape. The laser-weld bead dimensions are 1.78 mm wide and 2.93 mm deep, with a maximum width of 0.6 mm in the heat-affected zone. Some small pores appear in the laser weld bead, but adjacent to the joint, as in the GMAW case. The free surface of the bottom sheet does not exhibit a notch, as shown in **Figure 1(a)**.

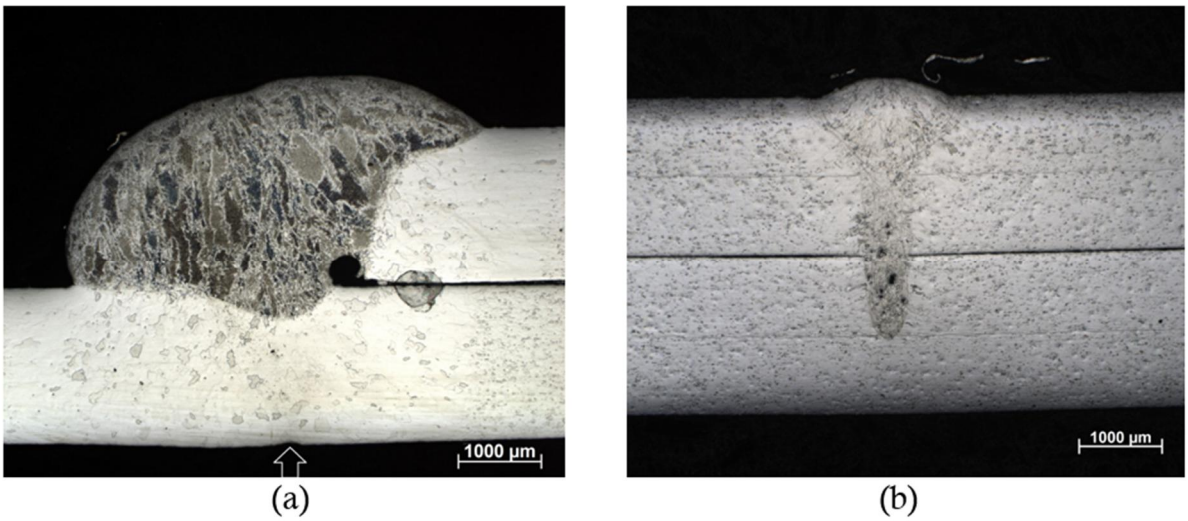

Figure 1. Optical micrographs of **(a)** GMAW and **(b)** LBW welds. The arrow indicates the notch at the bottom surface of the component.

Figure 2 shows two typical microstructures observed in the fusion zone (FZ) of the weld beads. The GMA weld beads (**Figure 2(a)**) were marked by the wire composition because the dilution of the base material was relatively low (**Figure 1(a)**). GMAW is characterized by grain boundaries, acicular ferrites, and pearlite in the middle of the grains (**Figure 2(a)**), in accordance with Boumerzoug et al.[9] and Bodude and Momohjimoh[10]. The laser beam-welded FZ (**Figure 2(b)**) presented ferritic (light gray) and pearlite (dark gray) grains, which also corroborates the literature[11,12].

Table 1 presents the average Vickers hardness (HV) values for the base material (BM), heat-affected zone (HAZ), and fusion zone (FZ) for different types of weld beads. The hardness of the base metal increased in the HAZ and FZ of the GMAW as a result of grain refinement. In the LBW case, the HV slightly increased in the FZ and HAZ because of the grain size.

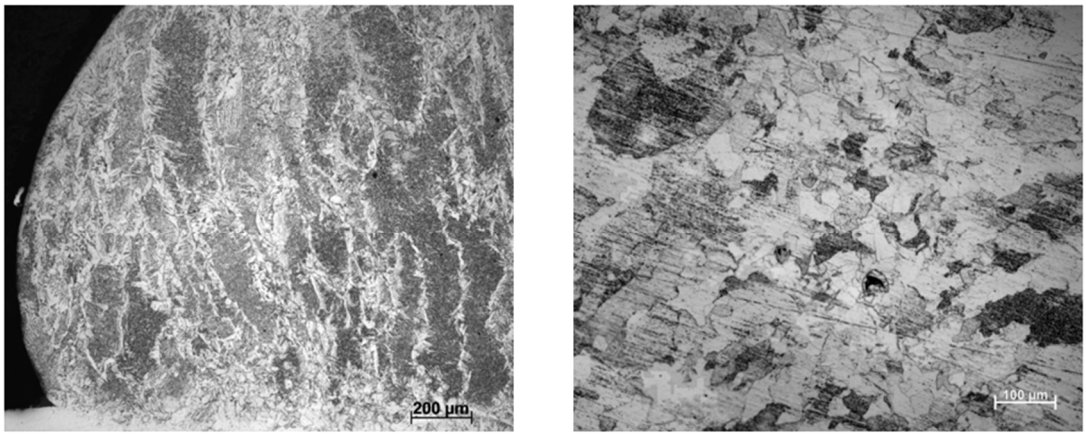

Figure 2. Optical microscopy images of the center of the fusion zone for **(a)** GMAW and **(b)** LBW.

Table 1. Hardness values for each region of the welds.

Region	GMAW	LBW
BM	100 ± 10	100 ± 10
HAZ	140 ± 10	110 ± 20
FZ	140 ± 10	150 ± 10

The stress-strain curves for a representative lap joint-type tensile test are presented in **Figure 3**. The shape and maximum strain points did not change significantly between the three tests under the same conditions. The maximum strengths of the LBW and GMAW coupons were 415 MPa and 84 MPa, respectively. In contrast, the maximum strains obtained for LBW and GMAW were 2.6% and 7.9%, respectively. In terms of toughness moduli, given by the area under the curves, LBW and GMAW are 2.9 MPa and 0.9 MPa, respectively.

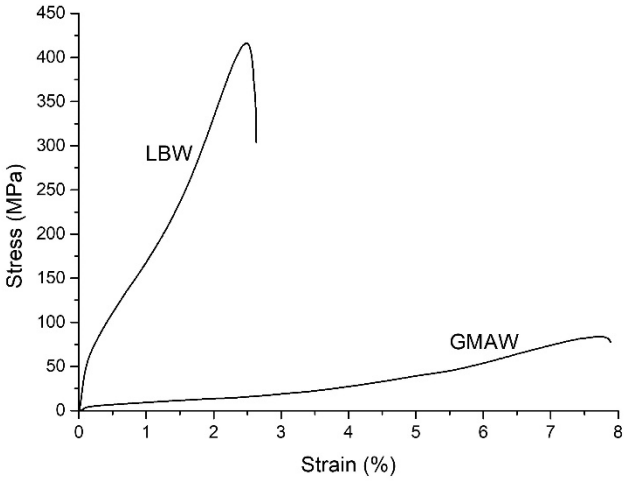

Figure 3. Lap-joint shear stress-strain curves representative of the LBW and GMAW samples.

The temperature profile in the middle of the welding process is shown in **Figure 4**. As can be seen, the GMAW case distributes the arc energy through a large portion of the component. For example, the temperature at the bottom of the lower sheet was 1200 °C in the GMAW case compared to the ambient temperature of the LBW case. The simulated dimensions of the melt pool (red areas in **Figure 4**) resemble the actual welds in both cases (**Figure 1**). Heat-affected zones (HAZ) are less visible because of the

ferritic base material. However, the presence of grain growth around the fusion region, as shown in **Figure 1(a)**, is indicative of the HAZ. Comparing **Figure 1(a)** and **Figure 4(a)**, it can be considered that the HAZ extends to approximately 1200 °C. This temperature was reported by Thaulow et al.[13] around the grain growth HAZ in low-carbon steels. The HAZ in the LBW case was much narrower than that in the GMAW case, approximately 300 μm in the optical micrograph (**Figure 1(b)**), giving approximately 700 °C in the simulated cross section (**Figure 4(b)**). This temperature was reported to be approximately equal to the A1 temperature of low-carbon steel[14]. In the literature by Oh et al.[15], these temperatures were sufficient to produce a hard and brittle HAZ composed of martensite. However, the very low carbon content kept the hardness level (**Table 1**) compatible with ferritic grains in the HAZ.

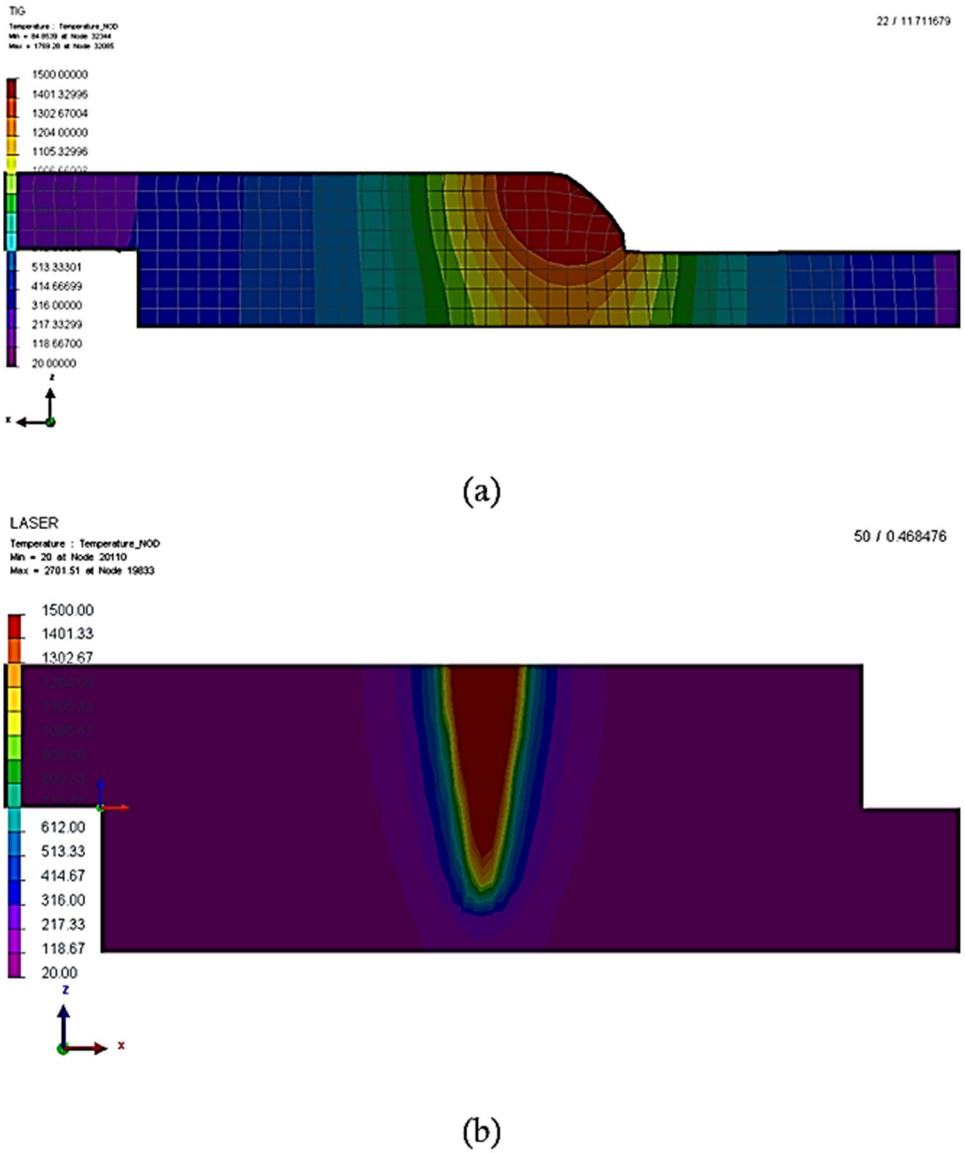

Figure 4. Temperature profiles for GMAW and Laser welds in the middle of the component.

From a thermomechanical point of view, **Figure 5** presents the Von Mises residual stresses for GMAW and LBW, as estimated from the upper free surface. The maximum residual stresses were approximately 220 MPa and 470 MPa for GMAW and LBW, respectively. Although the LBW stresses doubled the GMAW case, the laser beam weld confined the highest values, and the GMAW spread the stress lines far from the joint. As a result, the final displacement of the FEA mesh was much more

perceptible in the GMAW case than in the LBW case (**Figure 6**). In particular, a notch on the opposite face of the weld was visible in the GMAW simulation (**Figure 6(b)**). In the simulations, the volume was free to expand, and the notch was presented as a protuberance at the lower surface of the component (**Figure 6(b)**). This is exactly the inverse of the experimental evidence (arrow in **Figure 1(a)**) because, under real conditions, the sheets are not free to expand. Consequently, residual strain notches the surface at the bottom.

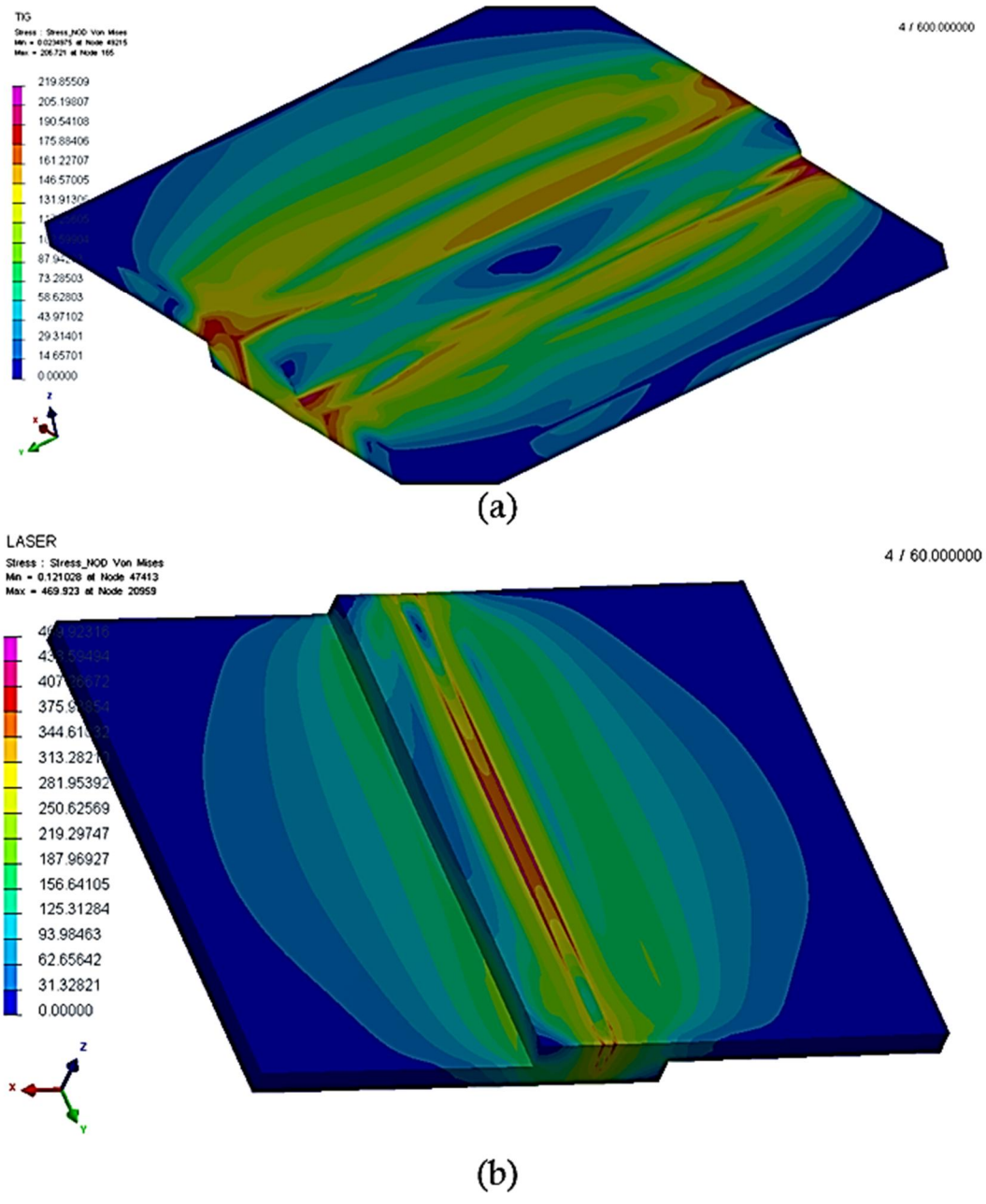

Figure 5. Von Mises stresses at the end of the simulation for **(a)** GMAW and **(b)** LBW.

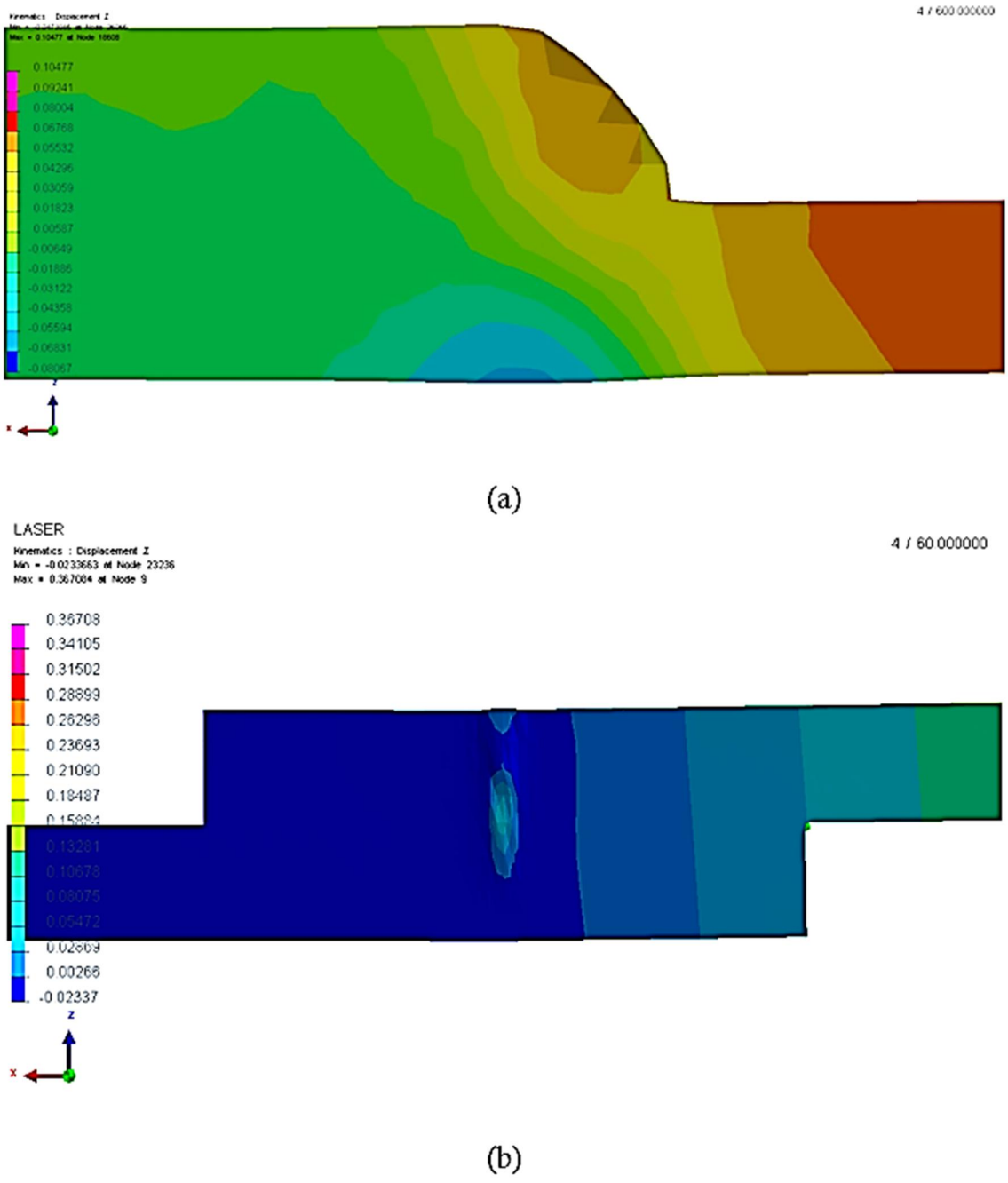

Figure 6. Final displacement of nodes in Z-direction (orthogonal to weld line) for **(a)** GMAW and **(b)** LBW.

4. Conclusions

The following conclusions were drawn:

Gas-metal arc welding (GMAW) and laser beam welding (LBW) were performed for superposed sheets of low-carbon steel.

The microstructures of the fusion zone are ferritic (LBW) or ferritic-pearlitic (GMAW), because the latter accounts for wire dilution.

The surface opposite the GMAW presented a notch as a visible defect, which was not present in the LBW.

The hardnesses of the base material, heat-affected zone, and fusion zone were similar (100–150 HV) owing to the majority of ferrite grains.

In terms of lap-shear tensile strength, LBW coupons were stronger (415 MPa) than GMAW coupons (84 MPa), but with a reduction in the final elongation from 7.9% to 2.6%.

Finite element analysis (FEA) indicated that the lateral heat exchange for GMAW was excessive, attaining 1200 °C at the face opposite to the weld. In the case of LBW, the opposite surface was maintained at room temperature.

The mechanical results of the FEA indicated a high von Mises maximum residual stress for LBW compared with GMAW. However, residual stresses were confined to the weldment. Owing to the intense heat input and residual stress, the GMAW presented a defect on the opposite surface.

Author contributions

Conceptualization, MSFdL; methodology, RHMdS; software, MSFdL; formal analysis, SMdC; investigation, MSFdL, SMdC and RHMdS; data curation, SMdC and RHMdS; writing—original draft preparation, MSFdL; writing—review and editing, SMdC; visualization, RHMdS; supervision, MSFdL; project administration, MSFdL; funding acquisition, MSFdL. All authors have read and agreed to the published version of the manuscript.

Acknowledgments

The authors acknowledge the São Paulo State Foundation (FAPESP) for financial support.

Conflict of interest

No conflict of interest was reported by all authors.

References

1. Hong KM, Shin YC. Prospects of laser welding technology in the automotive industry: A review. *Journal of Materials Processing Technology* 2017; 245: 46–69. doi: 10.1016/j.jmatprotec.2017.02.008
2. Baratzadeh F, Tay YY, Patil S, Lankarani HM. An experimental and numerical investigation into the dynamic crash testing of vehicle bumper fabricated using friction stir welding and gas metal arc welding. *International Journal of Crashworthiness* 2014; 19(4): 371–384. doi: 10.1080/13588265.2014.904062
3. Sakai PR, Lima MSF, Fanton L, et al. Comparison of mechanical and microstructural characteristics in maraging 300 steel welded by three different processes: LASER, PLASMA and TIG. *Procedia Engineering* 2015; 114: 291–297. doi: 10.1016/j.proeng.2015.08.071
4. Antunes WD, de Lima MSF. Experimental development of dual phase steel laser-arc hybrid welding and its comparison to laser and gas metal arc welding. *Soldagem & Inspeção* 2016; 21(3): 379–386. doi: 10.1590/0104-9224/SI2103.12
5. Hashemzadeh M, Chen BQ, Guedes Soares C. Comparison between different heat sources types in thin-plate welding simulation. In: Soares G, Peña L (editors). *Developments in Maritime Transportation and Exploitation of Sea Resources*. Taylor & Francis Group; 2014. pp. 329–335.
6. Derakhshan ED, Yazdian N, Craft B, et al. Numerical simulation and experimental validation of residual stress and welding distortion induced by laser-based welding processes of thin structural steel plates in butt joint configuration. *Optics & Laser Technology* 2018; 104: 170–182. doi: 10.1016/j.optlastec.2018.02.026
7. Pavan AR, Arivazhagan B, Vasudevan M, Sharma GK. Numerical simulation and validation of residual stresses and distortion in type 316L(N) stainless steel weld joints fabricated by advanced welding techniques. *CIRP Journal of Manufacturing Science and Technology* 2022; 39: 294–307. doi: 10.1016/j.cirpj.2022.08.010
8. ESI Group. Sysweld. Available online: https://www.esi-group.com/products/sysweld (accessed on 15 December 2023).
9. Boumerzoug Z, Derfouf C, Baudin T. Effect of welding on microstructure and mechanical properties of an industrial low carbon steel. *Engineering* 2010; 2(7): 502–506. doi: 10.4236/eng.2010.27066

10. Bodude MA, Momohjimoh I. Studies on effects of welding parameters on the mechanical properties of welded low-carbon steel. *Journal of Minerals and Materials Characterization and Engineering* 2015; 3(3): 55220. doi: 10.4236/jmmce.2015.33017
11. Yilbas BS, Arif AFM, Aleem BJA. Laser welding of low carbon steel and thermal stress analysis. *Optics & Laser Technology* 2010; 42(5): 760–768. doi: 10.1016/j.optlastec.2009.11.024
12. Deng D. FEM prediction of welding residual stress and distortion in carbon steel considering phase transformation effects. *Materials & Design* 2009; 30(2): 359–366. doi: 10.1016/j.matdes.2008.04.052
13. Thaulow C, Pauuw AJ, Guttormsen K. The heat affected zone toughness of low carbon microalloyed steels. *Metal Construct* 1985; 17(2): 94–99.
14. Zhang W, Roy GG, Elmer JW, DebRoy T. Modeling of heat transfer and fluid flow during gas tungsten arc spot welding of low carbon steel. *Journal of Applied Physics* 2003; 93(5): 3022–3033. doi: 10.1063/1.1540744
15. Oh HS, Kang J, Tasan CC. Enhancing damage-resistance in low carbon martensitic steels upon dual-pass laser treatment. *Scripta Materialia* 2021; 192: 13–18. doi: 10.1016/j.scriptamat.2020.09.047